Modeling of basal plane dislocations in single-crystal sapphire

Gao, Bing
Research Institute for Applied Mechanics, Kyushu University

Kakimoto, Koichi
Research Institute for Applied Mechanics, Kyushu University

https://doi.org/10.15017/1526335

出版情報：九州大学応用力学研究所所報. 148, pp.1-6, 2015-03. Research Institute for Applied Mechanics, Kyushu University
バージョン：
権利関係：

Modeling of basal plane dislocations in single-crystal sapphire

Bing Gao*, Koichi Kakimoto

E-mail of corresponding author: *gaobing@riam.kyushu-u.ac.jp*

(Received January 10, 2015)

Abstract

The Alexander–Haasen model was originally used to model the multiplication of the mobile dislocations in crystalline silicon. Here, we extend this model for studying multiplication of basal plane dislocations (BPDs) in single-crystal sapphire. By fitting the Alexander–Haasen model to experimental data, we find that the model accurately describes the plastic deformation of sapphire caused by BPDs. The application of the Alexander–Haasen model to sapphire growth made it possible to minimize the dislocation density and residual stress in growing crystals by optimizing the furnace structure and operation conditions. We apply the Alexander–Haasen model to investigate the dynamical deformation of single-crystal sapphire during cooling process, and examine the effect of the cooling rate on the generation of BPDs and residual stress. Finally, we present the BPD distribution and discuss the main factor that influences the generation of BPDs.

Key words : Basal plane dislocations, single-crystal sapphire, Alexander-Haasen model, Minimize dislocation density and residual stress.

1. Introduction

Single-crystal sapphire has recently garnered significant attention as an important substrate material for fabricating gallium nitride light-emitting diodes (LEDs), which promise great energy savings over both incandescent and compact fluorescent lighting technologies. The market for such lighting is currently expanding at double-digit annual growth rates.[1] High-quality gallium nitride requires high-quality sapphire substrates. To enhance the quality of crystalline sapphire (Al_2O_3), the density of dislocations must be controlled and reduced.

To reduce the generation rate of dislocations during the growth of crystalline sapphire, a model that relates dynamic dislocation generation to the practical growth conditions is required. However, no such model, which can describe the plastic deformation of sapphire, currently exists. To address this shortfall, the dislocation density-based Alexander–Haasen (AH) model[2,3] which was originally used for crystalline silicon, is applied to crystalline sapphire. The AH model has been used extensively to understand the plastic deformation of elemental[4-6] and III–V compound semiconductors[7-8] over a wide range of temperatures and stresses. Recently, the AH model has been extended to IV–IV compounds such as SiC[9-11], and the simulated results agree well with experimental data. Applying the AH model[12-14] to the global modeling of crystal growth of elemental, III–V, and IV–IV compound semiconductors has resulted in an extraordinary optimization and reduction of dislocations in these materials. Thus, it would be very useful to determine whether the AH model can be extended to crystalline sapphire.

2. Determination of Alexander – Haasen parameters from experimental data

Experiments on the tensile deformation of sapphire[15] have been performed at various temperatures (1200 °C to 1700 °C) and strain rates (10^{-5} to 10^{-3} s−1). These experiments[15] confirmed that plastic slip occurs mainly in the {0001} basal slip plane and slip direction; the other slip planes, such as prismatic and pyramidal, have high activation energy. Therefore, in this study, we model only basal plane dislocations. We fit the AH model to the experimental stress–strain curves.[15] Details of the fitting procedure are explained as follows.

In this paper, the following notation is used: the slip direction is α ; in the slip direction α, the resolved shear stress is $\tau_{resolv}^{(\alpha)}$ and the plastic strain is $\varepsilon_{pl}^{(\alpha)}$; the Schmid factor is Φ ; the applied stress in the tensile system is τ_a, and the plastic strain along the tensile direction is ε_{pl}. The satisfied relationships are as follows:

$$\tau_{resolv}^{(\alpha)} = \Phi \tau_a \tag{1}$$

$$\varepsilon_{pl}^{(\alpha)} = \varepsilon_{pl} / \Phi \tag{2}$$

* Research Institute for Applied Mechanics, Kyushu University

Equations (1) and (2) are easily understood by considering energy relationships if the applied stress only causes plastic deformation in the direction. The strain energies should be the same, i.e.,

$$E=\frac{1}{2}V\tau_{resolv}^{(\alpha)}\varepsilon_{pl}^{(\alpha)}=\frac{1}{2}V\Phi\tau_a\varepsilon_{pl}/\Phi=\frac{1}{2}V\tau_a\varepsilon_{pl} \quad (3)$$

The apparent shear strain ε along the tensile direction can be calculated based on the displacement of the cross head of the tensile machine. The elastic strain ε_{el} along the tensile direction is as follows:

$$\varepsilon_{el}=\varepsilon-\varepsilon_{pl} \quad (3)$$

The applied stress τ_a is related to the elastic strain as follows:

$$\tau_a=\eta\varepsilon_{el}=\eta(\varepsilon-\varepsilon_{pl}) \quad (4)$$

where η is the elastic constant of total tensile system. The differential ratio of the applied stress to the apparent shear strain is as follows:

$$\frac{d\tau_a}{d\varepsilon}=\frac{\eta(d\varepsilon-d\varepsilon_{pl})}{d\varepsilon}=\eta(1-\Phi\frac{d\varepsilon_{pl}^{(\alpha)}}{d\varepsilon})=\eta(1-\Phi\frac{d\varepsilon_{pl}^{(\alpha)}/dt}{d\varepsilon/dt}) \quad (5)$$

According to the AH model, the plastic strain rate in the α slip direction is expressed as follows:

$$d\varepsilon_{pl}^{(\alpha)}/dt=N_m^{(\alpha)}v^{(\alpha)}b^{(\alpha)} \quad (6)$$

where $N_m^{(\alpha)}$ and $v^{(\alpha)}$ are the mobile dislocation density and the velocity of dislocations in the α slip direction, respectively, and $b^{(\alpha)}$ is the Burgers vector. The velocity of dislocations is given by

$$v^{(\alpha)}=k_0\tau_{eff}^{(\alpha)m}\exp(-\frac{Q}{k_BT}) \quad (7)$$

where k_0 and m are material constants, Q is the activation enthalpy of dislocations, k_B is Boltzmann's constant, T is the temperature in kelvin, and $\tau_{eff}^{(\alpha)}$ is the effective stress for dislocation multiplication in the α slip direction and is given by:

$$\tau_{eff}^{(\alpha)}=\left\langle\tau_{resolv}^{(\alpha)}-D\sqrt{N_m^{(\alpha)}}\right\rangle \quad (8)$$

where D is the hardening factor. Note that $\langle x\rangle=x$ if $x>0$ and $\langle x\rangle=0$ if $x\le 0$.

Substituting equations (1) and (7)–(9) into Eq. (6) gives

$$\frac{d\tau_a}{d\varepsilon}=\eta\left[1-\Phi\frac{N_m^{(\alpha)}k_0b^{(\alpha)}\left\langle\Phi\tau_a-D\sqrt{N_m^{(\alpha)}}\right\rangle^m}{d\varepsilon/dt}\exp(-\frac{Q}{k_BT})\right] \quad (9)$$

Equation (10) shows that the stress–strain curve is determined by the strain rate $d\varepsilon/dt$, the temperature T, the mobile dislocation density $N_m^{(\alpha)}$, the Schmid factor Φ, the applied stress τ_a, the elastic constant η of the tensile system, and the material constants k_0 and m. The stress–strain relationship is very complex and stems from a dynamical system that is affected by its history of plastic deformation.

To close the system of equations, the AH model gives the following rate equation for the mobile dislocation density:

$$\begin{aligned}\frac{dN_m^{(\alpha)}}{dt}&=K\tau_{eff}^{(\alpha)\lambda}N_m^{(\alpha)}v^{(\alpha)}\\&=Kk_0N_m^{(\alpha)}\left\langle\Phi\tau_a-D\sqrt{N_m^{(\alpha)}}\right\rangle^{\lambda+m}\exp(-\frac{Q}{k_bT})\end{aligned} \quad (10)$$

where K and λ are material constants.

The model parameters in equations (10) and (11) are obtained by a fitting process that minimizes the target function $f=\sum\left|\tau_{a,experiment}(\varepsilon_i)-\tau_{a,numerical}(\varepsilon_i)\right|$ using the downhill simplex method.[16] Five experimental stress–strain curves[15] acquired at temperatures ranging from 1200 °C to 1700 °C were globally fit. The values obtained from the fit for the AH parameters are as follows:

$$k_0=1.084\times10^{-8},K=1.660\times10^{-3},\lambda=0.939,$$

$$m=3.000,\ Q=4.709\ (eV). \quad (11)$$

Figure 1 shows the comparison between the fit numerical results and the experimental data. The symbols and the smooth curves denote the experimental data and the fit numerical results, respectively. The experimental data are well fit by the stress-strain curves obtained from the AH model. This result indicates that the AH model is valid for single-crystal sapphire.

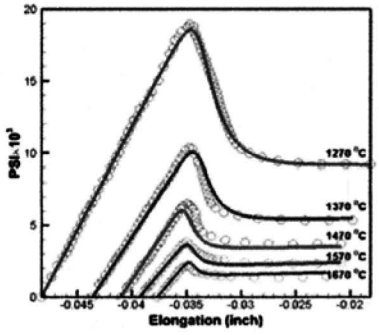

Fig. 1. Comparison between fit numerical results and experimental data at temperatures ranging from 1200 °C to 1700 °C for a strain rate of 1.667×10^{-6} s^{-1}. The symbols denote the experimental data, and the smooth curves denote the fit numerical results.

3. Application of the Alexander-Haasen model to sapphire cooling process

Now, we apply the AH model to track the rate-dependent process of plastic deformation during the cooling stage of the sapphire-growth process. The detailed calculations are quite similar to those for three-dimensional basal plane dislocations (BPD) in SiC.[9] An isotropic assumption of materials can be used and the elastic constant tensor matrix can be determined by Young's modulus and poisson's ratio; however, for incorporation of anisotropic effect, the elastic constant tensor matrix, which is determined by elastic constants[17] C_{11}, C_{12}, C_{13}, C_{33}, and C_{44}, can be used. The anisotropic stress calculation has to be solved in a three-dimensional system and it needs a lot of computational time. As pointed out in the paper[23,24], two simplifications can be done to reduce the total computational time with a small error of less than 6%. The first simplification is that the stresses $\sigma_{\theta z}$ and $\sigma_{r\theta}$ were considerably smaller than all other stress components and can be neglected[20-21]. The second simplification is that all of the terms involving trigonometric function of $n\theta$ can be neglected after the drop power transformation of trigonometric functions. Therefore, a simplified 2D stress-strain relation including thermal strain can be used to incorporate anisotropic effect[23,24].

The thermal expansion coefficient is set to 1.8×10^{-5} 1/K according to Ref. 22. For convenience, a table containing all parameters for simulation is provided in Table 1.

The primary target of this section is to test the AH model. Thus, to avoid complications, only the cooling process is investigated. The implementation and numerical results are given in the following sections.

Table 1. Parameters for the dislocation calculations.

	Description	Value or/and Units
b	Burgers vector in basal plane	4.76×10^{-10} (m)
K	Multiplication constant	1.660×10^{-3}
k_0	Material constant	1.084×10^{-8}
Q	Activation enthalpy	4.709
λ	Stress exponential factor	0.939
m	Stress exponential factor	3.0
k_b	Boltzmann constant	8.615×10^{-5} (eV/K)
C_{11}	Elastic constant	$-2.64\times10^{7}T+5.10\times10^{11}$ (Pa)
C_{12}	Elastic constant	$4.56\times10^{6}T+1.61\times10^{11}$ (Pa)
C_{13}	Elastic constant	$-6.22\times10^{6}T+1.15\times10^{11}$ (Pa)
C_{33}	Elastic constant	$-2.98\times10^{7}T+5.13\times10^{11}$ (Pa)
C_{44}	Elastic constant	$-1.96\times10^{7}T+1.57\times10^{11}$ (Pa)
β	Thermal expansion coefficient	1.8×10^{-5} (1/K)
D	Strain hardening factor	15.0
T	Temperature	K

3.1 Furnace Configuration and Targeted Temperature History

An axisymmetric and almost dislocation-free sapphire single-crystal ingot was first placed in an axisymmetric crucible. The initial BPD density was set to 1 cm^{-2} everywhere, which is quite low and does not influence the final dislocation density. The crystal axis was aligned in the [0001] direction. The crystal was 90 mm in diameter and 80 mm in height. The diameter of the crucible was 96 mm. A small gap of 3 mm between the crystal and crucible was maintained to accurately track dislocations by avoiding ambiguous boundary conditions between them. The bottom of crystal is taken to be free during the stress calculation. The basic configuration of the furnace18 around the crucible is shown in Figure 2. The furnace is used for a simple annealing process for testing the AH model.

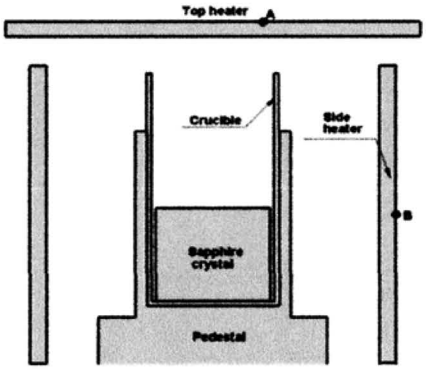

Fig. 2. The basic configuration of furnace around the crucible.

To determine how the cooling process influences the generation rate of dislocations, three different cooling processes were designed, as shown in Figure 3. In the high-temperature regime (greater than 1400 °C) of the cooling process, the cooling rates of cases 1, 2, and 3 were

different; however, the cooling rates of these cases were the same at low temperatures (less than 1400 °C). The heating process was the same in all three cases.

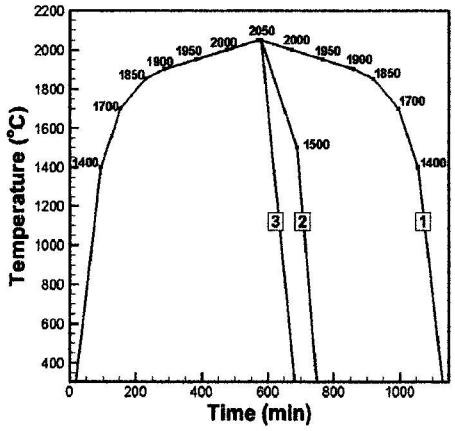

Fig. 3. Predesigned temperature history at monitoring points.

To homogenize the temperature distribution inside the furnace, we required the temperatures at two monitoring points (point A on the top heater and point B on the side heater, as shown in Figure 2) to be the same and to evolve as per the predesigned curves shown in Figure 3. To control the temperatures on the predesigned curves required, a nonlinear optimization algorithm was used to determine the heater power of the top and side heaters. A detailed numerical method for this is available in Reference 18.

3.2 Numerical Results for Dislocations

3.2.1 Dislocation Density Distribution Before and After Cooling

Gao et al.[14] showed that, for crystalline Si, the density of BPDs can dramatically increase during fast cooling; however, for crystalline SiC[9], the density of BPDs can decrease during fast cooling. How does cooling rate affect the generation of BPDs in sapphire?

Figure 4 shows the dislocation density distribution before and after cooling for case 3. Before cooling [Figure 4(a)], i.e., just after the heating process, the BPD density increases only at the bottom; however, after cooling [Figure 4(b)], the BPD density increases at both the bottom and at the side of the crystal. Therefore, the cooling process is a significant factor affecting the generation of BPDs during the growth of single-crystal sapphire.

Figure 5 shows the comparison of BPD density distributions for different cooling rates (cases 1–3). It is clear that the fastest cooling [Figure 5(c)] results in the largest BPD density, whereas the slowest cooling [Figure 5(a)] results in almost no increase in dislocation density relative to that before cooling [Figure 4(a)]. Because the main difference between cases 1–3 is the cooling rate in the high-temperature region, it is essential to use a slow cooling rate at high temperatures in order to reduce the rate at which dislocations are generated.

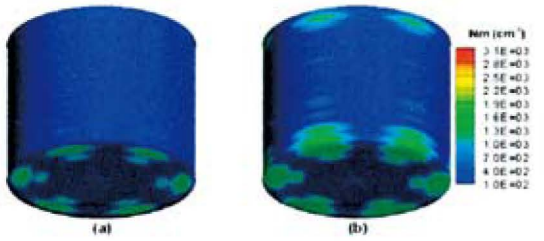

Fig. 4. The comparison of BPD distribution (a) before cooling and (b) after cooling for case 3.

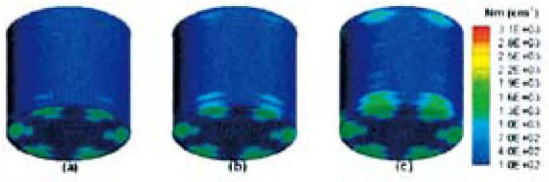

Fig. 5. The comparison of BPD distribution after cooling process for (a) case 1, (b) case 2, and (c) case 3.

Figure 4 shows that the dislocation density already becomes high at the bottom of crystal before cooling process. The possible reason is that the crystal directly touches the pedestal, through which the main outgoing cooling flux passes. Therefore, it is strong cooling flux causing high dislocation density at the bottom of crystal before cooling process starts.

3.2.2 Time Evolution of BPD and Residual Stress during Cooling Process

The main advantage of the Alexander–Haasen model is that it appropriately represents the rate-dependent process of plastic deformation in semiconductors or estimates the residual stress in cooled crystals. Figure 6 shows the time evolution of the BPD density in one slice taken from near the top of the crystal for cases 1 and 3. Figures 6(a1)–6(d1) is for case 1, and Figures 6(a2)–6(d2) is for case 3. During slow cooling [Figures 6(a1)–6(d1)], the dislocation density in the slice remains almost constant. However, during fast cooling [Figures 6(a2)–6(d2)], the dislocation density rapidly increases. Therefore, slow cooling helps to reduce the generation rate of dislocations.

After cooling, the von Mises residual stress inside the crystal can be obtained. Figure 7 shows the residual stress for three cooling schemes. The residual stress was averaged

along the peripheral direction, and thus, the planes in Fig. 7 pass through the axial line. The slowest cooling (case 1) corresponds to the lowest residual stress. As the cooling rate increases, the magnitude of residual stress gradually increases. Therefore, slow cooling helps reduce residual stress.

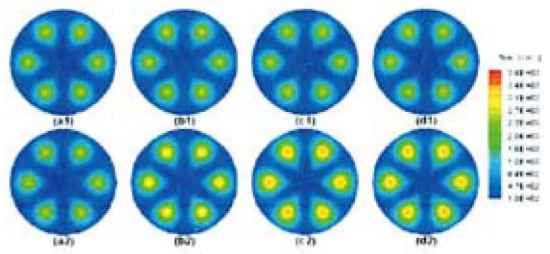

Fig. 6. Dislocation density distribution at different cooling times for case 1 [panels (a1)–(d1)] and for case 3 [panels (a2)–(d2)]. From panels (a) to (d) for both cases 1 and 3, the corresponding temperatures at monitored points are 2000 °C, 1950 °C, 1900 °C, and 1850 °C, respectively.

After cooling, the von Mises residual stress inside the crystal can be obtained. Figure 7 shows the residual stress for three cooling schemes. The residual stress was averaged along the peripheral direction, and thus, the planes in Fig. 7 pass through the axial line. The slowest cooling (case 1) corresponds to the lowest residual stress. As the cooling rate increases, the magnitude of residual stress gradually increases. Therefore, slow cooling helps reduce residual stress.

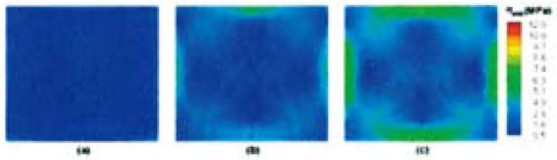

Fig. 7. Average residual stress in cooled crystal for (a) case 1, (b) case 2, and (c) case 3.

4. Conclusions

The Basal plane dislocations in single-crystal sapphire can be described by the Alexander–Haasen (AH) model. For the first time, the parameters of AH model for sapphire crystal have been derived from experimental stress-strain curves. The application of the Alexander–Haasen model to sapphire growth made it possible to minimize the dislocation density and residual stress in growing crystals by optimizing the furnace structure and operation conditions.

We applied the Alexander–Haasen model to crystals cooling in a small furnace. The results show that the cooling process significantly influences the generation rate of basal plane dislocations during the growth of single-crystal sapphire. Slow cooling rate from high temperature reduces the basal plane dislocation density and the residual stress.

References

1) Zhang, N.; Park, H. G.; Derby, J. J. J. Cryst. Growth 2013, 367, 27–34.
2) Haasen, P. Z. Phys. 1962, 167, 461–467.
3) Yonenaga, I.; Sumino, K. Phys. Stat. Sol. (a) 1978, 50, 685–693.
4) Sumino, K.; Yonenaga, I. Phys. Stat. Sol. (a) 1993, 138, 573–581.
5) Miyazaki, N.; Uchida, H.; Munakata, T. J. Cryst. Growth 1992, 125, 102–111.
6) Volkl, J.; Müller, G. J. Cryst. Growth 1989, 97, 136–145.
7) George, A.; Rabier, J. Rev. Phys. Appl. 1987, 22, 941–966.
8) Rabier, J.; George, A. Rev. Phys. Appl. 1987, 22, 1327–1351.
9) Gao, B.; Kakimoto, K. Cryst. Growth Des. 2014, 14, 1272–1278.
10) Gao, B.; Kakimoto, K. J. Cryst. Growth 2014, 386, 215–219.
11) Gao, B.; Kakimoto, K. J. Cryst. Growth 2014, 392, 92–97.
12) Miyazaki, N.; Okuyama, S. J. Cryst. Growth 1998, 183, 81–88.
13) Miyazaki, N.; Kumamoto, A.; Harada, C. J. Cryst. Growth 2004, 271, 358–367.
14) Gao, B.; Nakano, S.; Harada, H.; Miyamura, Y.; Kakimoto, K. Cryst. Growth Des. 2013, 13 2661–2669.
15) Kronberg, M. L. J. Am. Ceram. Soc. 1962, 45, 274–279.
16) Nelder, J. A.; Mead, R. Comput. J. 1965, 7, 308–313.
17) Dobrovinskaya, E. R.; Lytvynov, L. A.; Pishchik, V. Sapphire: Materials, Manufacturing, Applications, Science Bussiness Media, Springer, 2009.
18) Gao, B.; Kakimoto, K. J. Cryst. Growth 2014, 396, 7–13.
19) Garandet, J. P. J. Crystal Growth 1989, 96, 680–684.

20) Bottcher, K.; Cliffe, K. A. J. Cryst. Growth 2007, 303, 310–313.
21) Gao, B.; Nakano, S; Kakimoto, K. J. Cryst. Growth 2013, 369, 32–37.
22) Lu, C.W.; Chen, J. C. J. Cryst. Growth 2001, 225, 274–281.
23) Gao, B.; Nakano, S.; Harada, H.; Miyamura, Y.; Sekiguchi, T.; Kakimoto, K.; Cryst. Growth Des. 2012, 12, 5708–5714.
24) Lambropoulos, J. C. J. Cryst. Growth 1987, 84, 349–358.